IOPscience iopscience.iop.org

Home Search Collections Journals About Contact us My IOPscience

A hybrid of microreplication and mask-less photolithography for creating dual porosity and textured surface membranes

This content has been downloaded from IOPscience. Please scroll down to see the full text.

2013 J. Micromech. Microeng. 23 117005

(http://iopscience.iop.org/0960-1317/23/11/117005)

View the table of contents for this issue, or go to the journal homepage for more

Download details:

IP Address: 129.137.183.247
This content was downloaded on 08/01/2014 at 20:31

Please note that terms and conditions apply.

IOP PUBLISHING JOURNAL OF MICROMECHANICS AND MICROENGINEERING

J. Micromech. Microeng. **23** (2013) 117005 (8pp) doi:10.1088/0960-1317/23/11/117005

TECHNICAL NOTE

A hybrid of microreplication and mask-less photolithography for creating dual porosity and textured surface membranes

M Hagedon and J Heikenfeld

University of Cincinnati, Cincinnati, OH, USA, Cincinnati

E-mail: heikenjc@ucmail.uc.edu

Received 4 March 2013, in final form 5 September 2013
Published 21 October 2013
Online at stacks.iop.org/JMM/23/117005

Abstract

Microporous membranes have a number of applications in microfluidic devices including biotechnology and displays (Hagedon *et al* 2012 *Nature Commun.* **3** 1173, De Jong *et al* 2006 *Lab Chip* **6** 1125–39). Though commercially available micro-porous membranes are widely available using the ion track-etch method, there are few economical techniques to make mechanically robust membranes with dual pore sizes and/or surface texture. We demonstrate fabrication of high strength polyamide (poly(p-phenylene-2,6-benzobisoxazole)) membranes using a hybrid microreplication and mask-less photolithographic method. The fabricated films are only ∼6–10 μm thick, yet adequately strong to be released and handled with diagonals of at least several inches. The films contain dual pore sizes (32 μm, 6 μm) with the smaller pores achieving 1:1 aspect ratio, and the films include a highly-engineered surface texture. These films are demonstrated in application for electronic-paper displays, and exhibit robust optical switching and diffuse (paper-like) reflectance.

(Some figures may appear in colour only in the online journal)

1. Introduction

Microporous membranes have wide reaching applications including separation, filtration, and protein patterning [3]. In some applications precise pore size and location are desirable but remain difficult using traditional membrane fabrication techniques such as ion track etching [4, 5]. In order to create a highly engineered membrane, one must look to micro and nanofabrication techniques used in today's semiconductor industry [6]. Examples such as micro-sieves enable extremely small precise features but are high cost per unit area. Furthermore, many of the conventional materials used for microporous membranes are not compatible with integration of electronic or other functional materials.

Membrane fabrication by microreplication is rarely used, despite the advantages of the process including simultaneously forming multiple features, heights, and textures using low cost and large scale production. The primary difficulty for microreplicating membranes is in creating the through holes. Through hole formation requires removal of residual polymer layers after or during the microreplication process. The problem has been explored and has been partially solved through a number of means, including post processing with reactive ion etching and specially formed molds which fracture the residual layer [7]. A simpler yet higher-resolution process would enable broader adoption of microreplication for microporous membrane fabrication.

In addition to conventional applications for microporous membranes, a recent paper written by our group has identified the application of polymer microporous membranes to create high performance reflective displays (electronic-paper or 'e-paper') [1]. This new display technology has been referred to

 © 2013 IOP Publishing Ltd Printed in the UK & the USA

as a microfluidic imaging film. The film relies on an optically reflective membrane which is able to simultaneously transport colored polar fluid and transparent non-polar fluid opposite directions. To achieve this, the membrane must contain two pore types of different sizes, one which always transports polar fluids and one which always transports non-polar fluids. For the purposes of demonstrating the device, the original paper used a fabrication technique which relies on a combination of ion track etching and reactive ion etching to achieve a membrane with multiple pore sizes. However, this fabrication approach is costly, and incapable of transferring surface texture to a membrane which, in e-paper, enables diffuse (paper-like) reflection. These challenges provided our motivation to find a simplified technique to create microporous membranes for e-paper applications.

We report here, an entirely new and improved microporous membrane fabrication technique. The highly unique and enabling process uses a novel combination of a cast-and-cure microreplication with mask-less photolithography to create a microporous membrane with dual porosity (~32 μm, ~6 μm) and a surface microtexture designed for optimal light scattering (the physical features required for a microfluidic imaging film). To accomplish this, a specialized polymer mold with high UV transmission is created which enables direct UV exposure of a positive photoresist above the raised mold features (inverse of the through holes). The full exposure of the remaining membrane material is blocked by the thick, highly UV absorbing photo resist. This results in fully cleared through holes after the membrane is released from the mold. Although the membranes fabricated here have been designed and demonstrated for use in e-paper applications, other applications can potentially benefit from the ability to use a microreplication process to fabricate microporous membranes with tight control of pore size, shape, and distribution, and the option for surface texturing.

2. Fabrication

There are two major fabrication processes in creating the membrane: first the mold fabrication; second, use of the mold for fabrication of the membrane. Here we describe the fabrication steps in order starting with the mold and finishing with the membrane. In the discussion at the end, justification will be provided for the chosen process steps and material. As this paper reports a new fabrication process, the following descriptions of the fabrication contain the major results and findings of this work.

2.1. Mold fabrication

The mold fabrication process is shown in figures 1(*a*)–(*e*) and requires multiple steps because of the multi-featured requirements of the membrane. First, the textured reflector patterns are microreplicated in SU-8 using a PDMS daughter mold with several minor modifications compared to the conventional process [8]. A 5 to 1 mixture of Sylgard 184 poly(dimethylsiloxane) (Dow chemical) precursor and activator was poured over a Ni master mold containing the micro textured surface to be transferred to the final membrane. The mold and PDMS were degassed under vacuum for 30 min at 20 m Torr. The PDMS was then cured at 100 °C for 30 min before being removed from the Ni master mold.

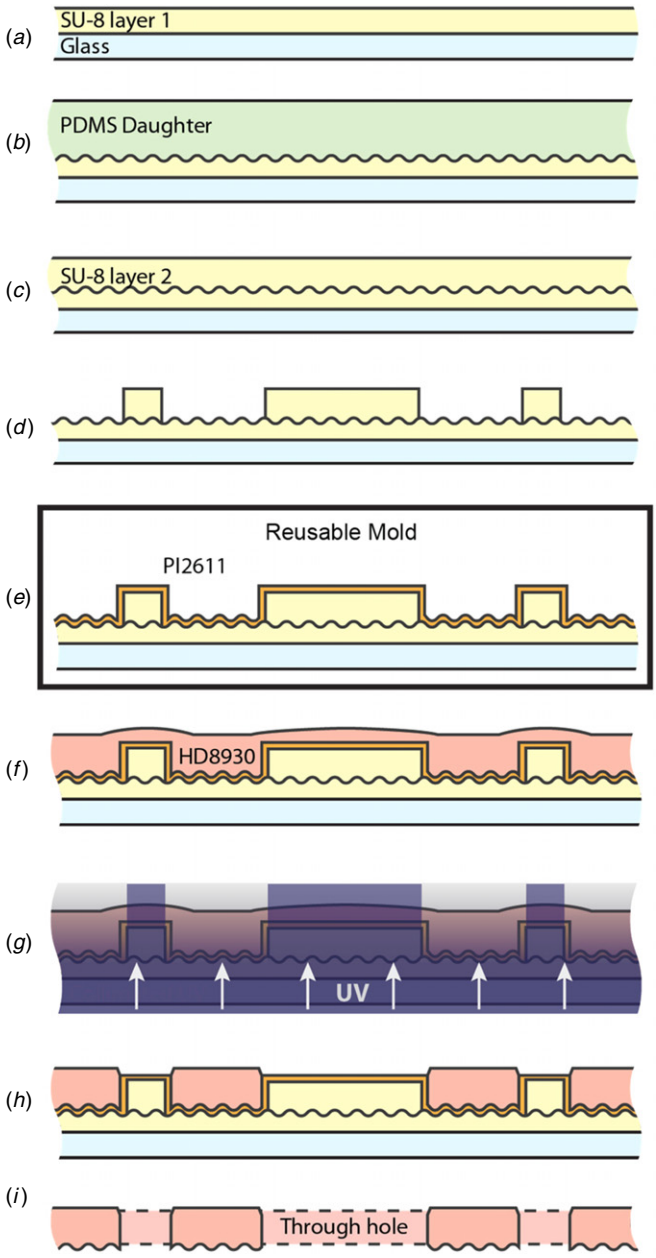


Figure 1. Fabrication process of the reusable mold: (*a*) SU-8 spin-coated on glass (*b*) hot embossing of PDMS daughter into SU-8 (*c*) second layer of SU-8 spun coat over the first layer of SU-8 containing diffuser pattern (*d*) SU-8 post field patterned by photolithography (*e*) reusable mold with spin-coated PI2611 release layer applied and cured. Fabrication of the HD8930 membrane: (*f*) HD8930 spin-coated over the mold from (*e*) and (*g*) backside UV illumination with light transmission through raised features (*h*) development of HD8930 to remove material on top of raised features (*i*) film released from mold using thermal release tape.

Next, a glass substrate was prepared with a solvent rinse followed by an oxygen plasma clean. MicroChem SU-8 2000 series was spin-coated on the substrate to a thickness of 5 μm (figure 1(*a*)). An extended solvent bakeoff of 30 min at 100 °C

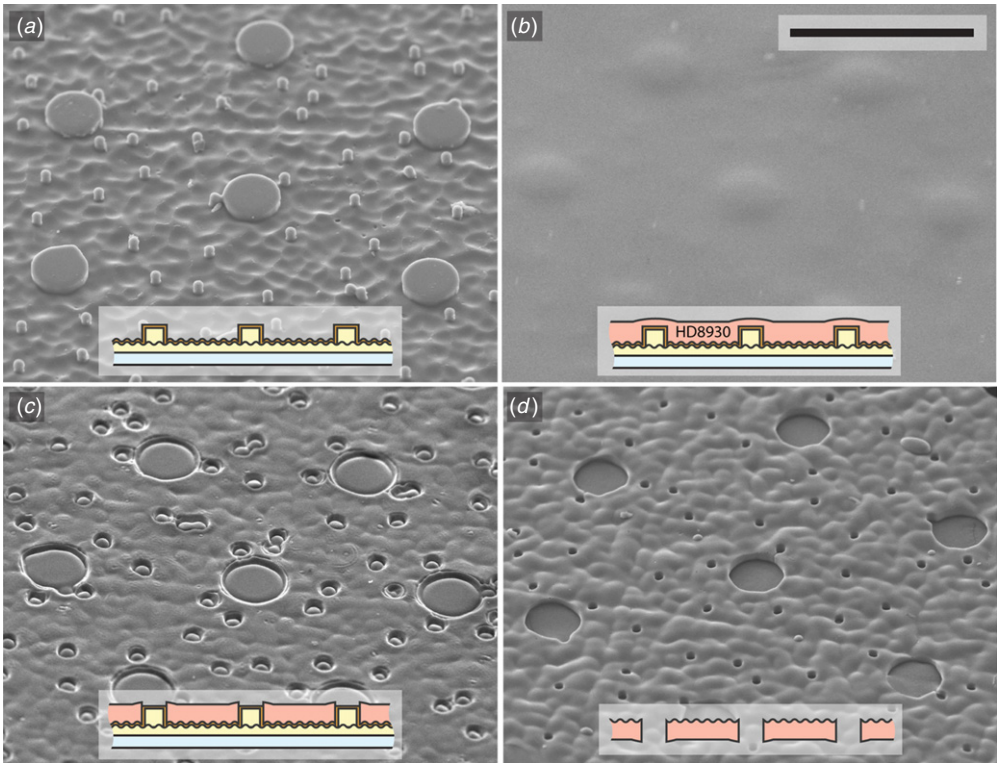


Figure 2. Scanning electron microscope images of the (*a*) SU-8 mold coated with a PI2611 release layer, (*b*) after being spin-coated with HD8930, (*c*) and after backside UV exposure and development. (*d*) The released membrane with an example of a microstructured surface. Scale bar 100 μm.

was used to remove all residual solvents from the SU-8 layer. The textured PDMS mold was then applied to the SU-8 layer and laminated using a hot roll laminator (XRL-120, Western Magnum). The laminator was adjusted such that the SU-8 was taken above its non-cross-linked melting point of 55 °C, and hot embossed with a roller pressure of 10 PSI (adequate to remove all air bubbles). The SU-8/PDMS stack was then exposed to 150 mJ cm^{-2} of i-line filtered UV light. A 5 min post-exposure bake was performed with the PDMS mold still in place to complete cross-linking of the SU-8. The SU-8/PDMS stack was then cooled to room temperature and the PDMS mold removed leaving the microreplicated diffuse reflector pattern on the SU-8 surface.

Onto this reflector-textured SU-8 layer, a second layer of SU-8 was spin-coated to a thickness of 8.6 μm measured using a Dektak 3030 mechanical profilometer. This second layer of SU-8 was patterned by manufacturer-standard SU-8 UV lithography and chemical development to create the inverse pattern of the desired membrane pores (figure 1(*d*)). Photolithography performed on a textured surface will typically result in decreased resolution due to scattered light off of the underlying surface. In this case however, the index of refraction of the uncured photoresist is well matched to the underlying surface material (cured photoresist) at the i-line wavelength, therefor effectively no resolution loss is observed and high fidelity SU-8 structures can be formed. It should be noted that this SU-8 photolithography step could be eliminated in the future by integrating the pore features into the Ni master mold allowing them to be microreplicated into the SU-8 simultaneously with the surface microtexture. After development in propylene glycol monomethyl ether acetate, the substrate and SU-8 features were then hard-baked at 180 °C for 30 min to fully cure the SU-8 and make it resilient to subsequent fabrication processes. After hard-bake, the SU-8 was exposed to a low-power O2 plasma treatment (4 W cm^{-2}, 30 s, 10 Torr) to improve the SU-8 surface's ability to bond to a subsequent thin polyimide coating.

A thin polyimide coating is added to act as a low adhesion layer, specifically for the mechanical release of molded polyamide. PI2611 was recommended by the HD Microsystems as a release layer due to its compatibility for spin casting of HD8930 and low adhesion to the HD8930 after curing. This mold release layer was spin-coated with PI2611, diluted to a 1:3 concentration with n-methyl-pyrollidone, spin-coated at 5000 rpm for 30 s, and baked at 260 °C for 60 min in an N2 environment, resulting in a ∼50 nm thick mold release layer. This is under the recommended PI2611 cure temperature of 350 °C, but was found to be fully sufficient for subsequent release of the membrane. At this point in the process, a reusable mold was complete (figure 1(*e*)), containing all the features necessary for replicating the highly sophisticated membrane in a single, mask-less photolithography step.

2.2. *Membrane fabrication*

A diagram of the membrane fabrication process is shown in figures 1(*f*)–(*i*). Scanning electron microscope images of the membrane at each step of the process are shown in figure 2.

A positive PBO (poly(p-phenylene-2,6-benzobisoxazole)) photoresist (HD8930, HD microsystems), was spin-coated at 2000 rpm for 30 s, to a measured thickness of 9.3 μm on the mold, then baked on a leveled hotplate for 180 s at 120 °C (figures 1(*f*) and 2(*b*)). The raised areas seen in figures 1(*f*) and 2(*b*) are due to the post features on the mold. The heights of the protrusions over the 32 μm and 6 μm posts were measured to be 2.3 μm and 0.5 μm respectively corresponding to a total of 3.0 μm and 1.2 μm of HD8930 above the post features. The back side of the mold was then exposed to 50 mJ cm^{-2} I-line filtered collimated UV light. The UV transmission of the SU-8 is much higher than the transmission of the uncured HD8930 which significantly increases the light exposure of the HD8930 above the SU-8 posts (figure 1(*g*)). The total exposure energy is far under the required dose for an 9.3 μm layer of HD8930, but is sufficient exposure for the development of the thin layer on top of the SU-8 posts. The HD8930 is then developed (puddle, 60 s) with 0.26N tetramethylammonium hydroxide solution, predominantly removing HD8930 coated over the posts, and leaving the under-exposed HD8930 membrane on the surface (figures 1(*h*) and 2(*c*). The membrane was then cured in an N2 environment at 180 °C for 120 min. The membrane was released from the mold by laminating a thermal release tape at room temperature followed by mechanical separation of the tape from the substrate. The thermal release tape carrying the membrane is then heated in a 120 °C oven for 5 min, reducing the adhesion such that the membrane can be separated using tweezers. The mold can be reused by cleaning the surface with acetone and annealing the PI2611 in a 260 °C oven for 20 min. The necessity of the cleaning and re-annealing step is not well understood, however the HD8930 does contain an integrated adhesion promoter which may be left behind after release from the mold. Cleaning and annealing likely removes this residue leaving a clean surface for re-use.

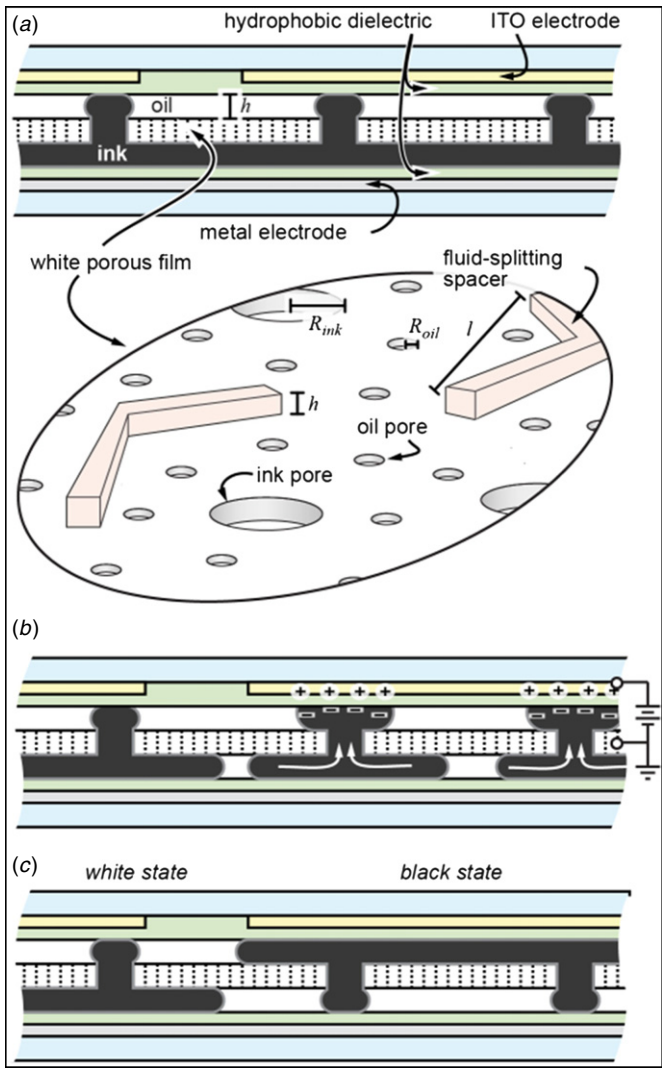


Figure 3. (*a*) Side view of the electrofluidic imaging film in its static off state with ink stable in the hidden (lower) channel. Additional important features are shown in the angled view diagram of the white film (lower panel). (*b*) Side view after voltage has been applied to one of the top electrodes to move ink and (*c*) after ink has merged in the visible channel the voltage is removed. Diagram adapted from [1].

3. e-paper display application

As mentioned in the introduction, the motivation for this work was to create a membrane which can be integrated into a specific display application presented in a previous report [1]. Here the operating principles of the membrane used in a display application are reviewed in order to reveal what factors are driving the design of the membrane in this specific work. Greater detail of display operation and design can be found in the previously published article.

3.1. Display device operating principles

As shown in figure 3(*a*), the device consists of a top and bottom channel of equal height separated by a membrane with aluminum coated micro-textured surface which causes light scattering giving a white paper-like appearance when in the reflective state. The device is filled with equal volumes of two fluids, a transparent non-polar fluid (oil) and an absorbing polar fluid (ink), which must then be transported across the reflective membrane to either hide or reveal the reflective surface of the membrane. The reflectance of the device is determined by the area of the reflective surface covered by ink. To transport the fluid between the two channels, dedicated fluid paths for each fluid phase are required. The fluid phase which is conducted through a given pore is determined by the geometry of the channel height and the pore radius which results in the need for multiple pore sizes ($R_{\text{pore}} > h \Rightarrow$ ink, $R_{\text{pore}} < h \Rightarrow$ oil) [1]. Therefore, the membrane is designed with a regular lattice of large pores for transporting the ink and a much denser array of smaller pores for transporting transparent non-polar fluid oil.

By applying an electric potential between the polar fluid and an electrode coated with a hydrophobic dielectric in one of the two channels, an electromechanical pressure, generated by electrowetting [9], pulls the polar fluid to the corresponding channel while the non-polar fluid is displaced into the other channel and breaks up the colored polar fluid sheet (figure 3(*b*)). When voltage is removed, the fluid merges

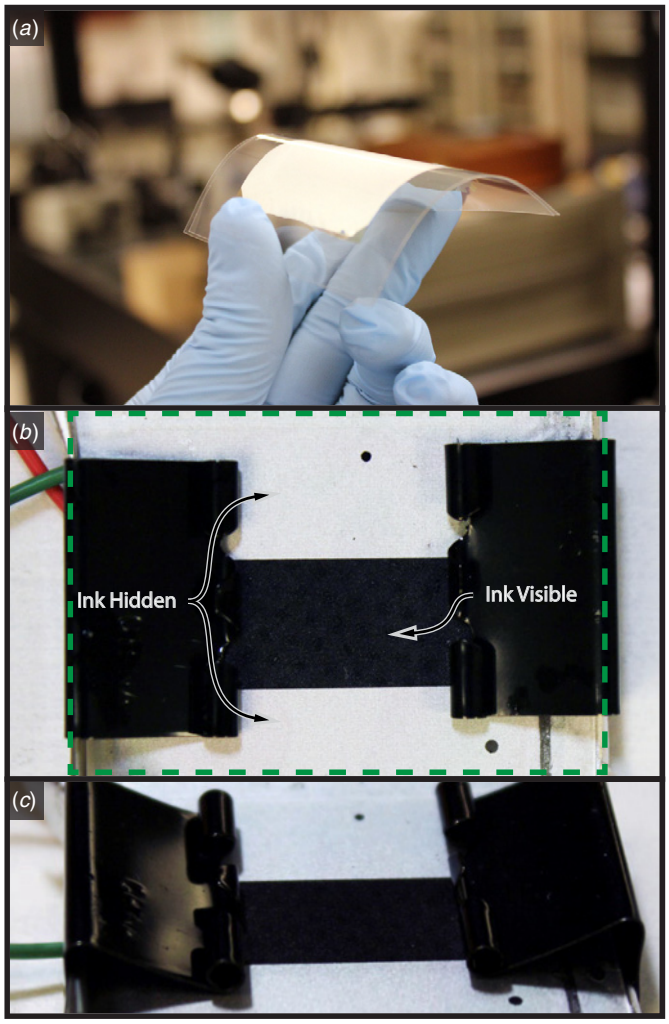


Figure 4. Photographs of a 2″ × 2″ microreplicated electrofluidic imaging film (*a*) flexed between two PET sheets filled with an oil, (*b*) in an rigid testing platform with a diffuse light source at 15 ° off normal and the camera at 0° off normal, (*c*) camera at 55° off normal. In (b) and (*c*) a white cotton sheet has been used as a background for comparison to the device. The device pictured is 1″ × 1″. The dashed, green bounding box in (*b*) denotes the device area.

and is stable in its position due to equal channel height and therefore equal pressure in both channels (figure 3(*c*)) [1, 10].

3.2. Device integration

In order to integrate the membrane into a display application, the released HD8930 membrane was coated on its textured side with 75 nm of evaporated aluminum to act as a reflector and a grounding electrode. This is followed by a dip coat of ∼100 nm of fluoropolymer (Fluoropel 1601 V, Cytonix Corp) and an annealing bake at 180 °C to provide the hydrophobicity required for display operation [1].

The reflective and non-reflective state of the resulting 1″ × 1″ device, actuated by a rectangular electrode, is shown in figures 4(*b*) and (*c*) as viewed at different angles to reveal the paper-like appearance of the textured membrane (diffuse reflection). The membrane texture, as seen in figure 2(*c*), has been designed to provide a diffuse white state while taking into account our previously reported requirements for efficient light out coupling [11]. The actual texture geometry is proprietary to Gamma Dynamics Corp., but such details are not important to this report because the fabrication process can create any surface texture that is compatible with typical microreplication techniques. Devices demonstrated in this work were not sealed prior to operation (simple clips were used, figures 4(*b*) and (*c*). The process for dosing and assembly of a sealed display module has been developed, but is proprietary information of Gamma Dynamics Corp.

3.3. Device performance and operation

The fully fabricated membrane was tested inside an unsealed display module (figure 4). The film was switched between white and black states with no significant difference in device switching times and fluidic behavior observed between the previous [1] and new fabrication process (this work). The film also successfully demonstrated a diffuse (paper-like) reflectance when assembled into a device. Figure 4(*a*) demonstrates the even brightness of the film while being flexed (paper like reflection). Figures 4(*b*) and (*c*) demonstrate the high contrast of the white and black states at varying angles. The white state reflectivity was measured using an integrating sphere and a spectrometer attached to a collimated fiber receiver [11]. The total white state reflectance was measured at 61% which is below the value from the previous report but still above the values reported by competing technologies [12]. This reflectance loss is seen due to increased light scattering which results in lower outcoupling efficiency (due to total internal reflection of scattered light at the glass/air interface) [11]. In this work, we have shown the fabrication and characterization of one diffuser design in order to demonstrate the fabrication process and a device with a paper-like reflectance distribution. To achieve a higher reflectance, further optimization of the reflector must be performed to balance increasing paper-like appearance with decreasing outcoupling efficiency. This optimization is outside the scope of this report, but has been explored in depth by Gamma Dynamics.

4. Discussion

4.1. Choice of HD8930 as the membrane material

The choice of membrane and mold materials is important to the success of this process as well as the integration of the membrane into a device. For integration with an electronic device, it is desirable to be compatible with processes used in the current flexible electronics industry. Polyimides are a standard material used in electronics as well as flexible electronics, and the material properties of polyimides (high strength, flexibility, temperature stability) align well with the requirements for the electrofluidic imaging film. However, microreplication in polyimides is difficult due to the high cure temperature (375 °C) and glass transition temperatures (>700 °C), as well as the use of highly polar solvents for polyimide precursors which swell most polymers that might be used as casting a mold [13]. No literature has been identified

which describes microreplicated through hole fabrication in polyimide. Polyamides such as those in the Nylon family have played a lesser role in the electronics industry to date, however poly(p-phenylene-2,6-benzobisoxazole) (PBO), has similar mechanical and thermal properties to polyimide but requires a lower curing temperature (170 °C) and the precursor contains a lower concentration of N-methyl-pyrollidone. For these reasons the photo-patternable PBO resist, HD8930, was chosen as the membrane material.

4.2. Mold requirements due to choice of HD8930

By selecting HD8930 as the membrane material, the microreplication mold material must meet certain criteria. Firstly, to enable the mask-less exposure process described in the membrane fabrication section, the material must have UV transmission much higher than that of uncured HD8930. Secondly, it must be stable up to 180 °C, and the material must be resistant to N-methyl pyrollidone which is a typical solvent found in PBO and polyimide precursors. Thirdly, it must be able to be fabricated into 3D structures either by microreplication or photolithography. These constraints are satisfied by the negative tone photoresist SU-8. Patterning SU-8 with optical structures, such as the diffuser required by this research, can be accomplished by a number of 3D greyscale lithography and microreplication techniques [14, 15]. To avoid bonding with the HD8930 and the SU-8 surface of the mold was coated with partially cured polyimide (PI2611) (260 °C). This also makes the mold surface highly recoverable by re-annealing. The high temperature of this anneal step can cause loss of UV transmission in the SU-8 layer over several repetitions of the process. Despite this, molds have been used successfully up to five times before the films have failed to develop correctly. To make the mold more robust, a lower cure temperature release layer should be used, or a replacement for the HD8930 used which does not foul the mold surface.

4.3. Fidelity of pore formation

The pore formation was monitored from at various stages of photoresist development using a SEM. The SEM micrographs shown in figures 2 and 5 clearly display the formation of the pores as the process was designed. Figures 5(*a*)–(*d*) show the posts being exposed as the residual layer of photoresist is developed. Due to the variation of thickness of the HD8930 above the two sizes of post features, the development of the 6 μm pores occurs much quicker than the development of the 32 μm pores.

Figures 5(*e*) and (*f*) show a comparison of the pore shape between the new process compared with a traditional mask based lithography process. When using traditional photolithography, the HD8930 creates conical pores due to the low resolution of the photoresist as well as the reflow of the photoresist during the HD8930 curing step. The high aspect ratio of the pores and low resolution of the resist also result in high variation of pore size due to small differences in exposure energy and film thickness over the substrate. This variation in the film can cause variation in device behavior across the display area and the conical pore shape can cause hysteresis

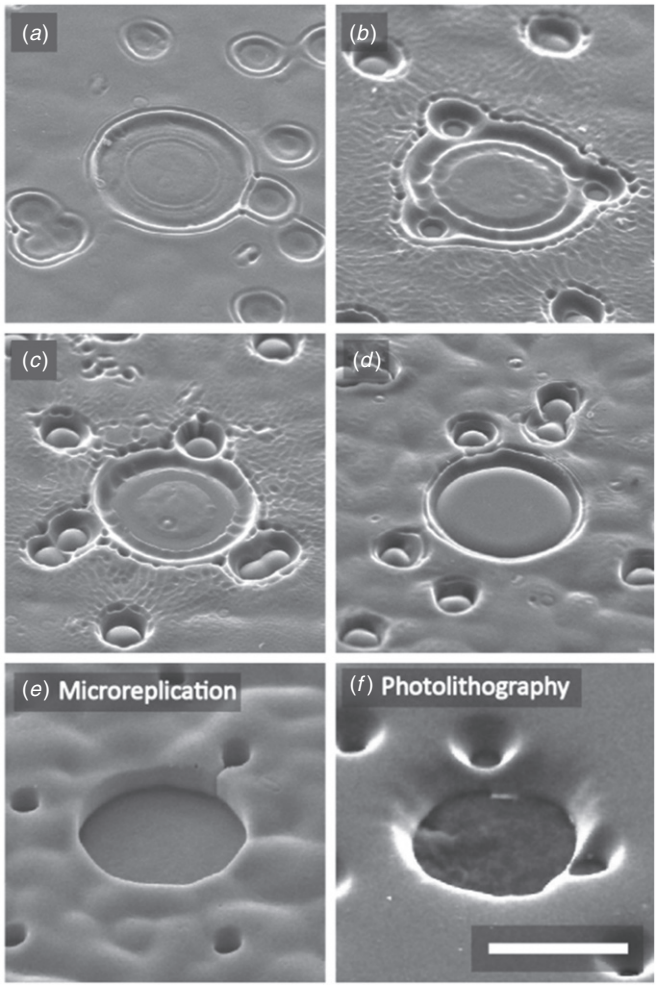


Figure 5. (*a*)–(*d*) The development of the HD8930 layer above the mold posts with (*a*) 30 s, (*b*) 45 s, (*c*) 60 s, and (*d*) 75 s of development time. (*e*) and (*f*) Comparison of pore shape using (*f*) traditional pholithography only and (*e*) using hybrid microreplication photolithography process. Scale bar 30 μm

in switching. The microreplication process we report here (figure 5(*e*)) achieves an improved side wall profile with a smaller variation in pore size. During the HD8930 curing step, the HD8930 reflows to conform to the side walls of the posts creating a highly cylindrical pore as seen in figure 5(*e*). These high fidelity pores guarantee that the fluid transport over the film is symmetric in both directions and uniform over the device area.

4.4. Fidelity of texture microreplication

As well as monitoring the process to confirm the proper formation of the pores, the transfer of the optical diffuser pattern was monitored through each step of the process. For these measurements, a membrane was fabricated without pores in order to eliminate error due to the optical effects of these features. The measurements were taken using a custom built gonioreflectometer diagramed in figure 6. The instrument measures the luminance of a substrate illuminated by a fixed directional source as the angle of the collimated receiver is rotated. The measurement setup is computer controlled

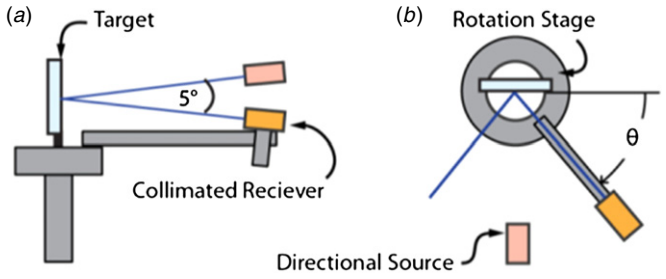


Figure 6. Diagram of measurement setup (*a*) side view (*b*) top view. Blue line is the specular sight line of the collimated receiver.

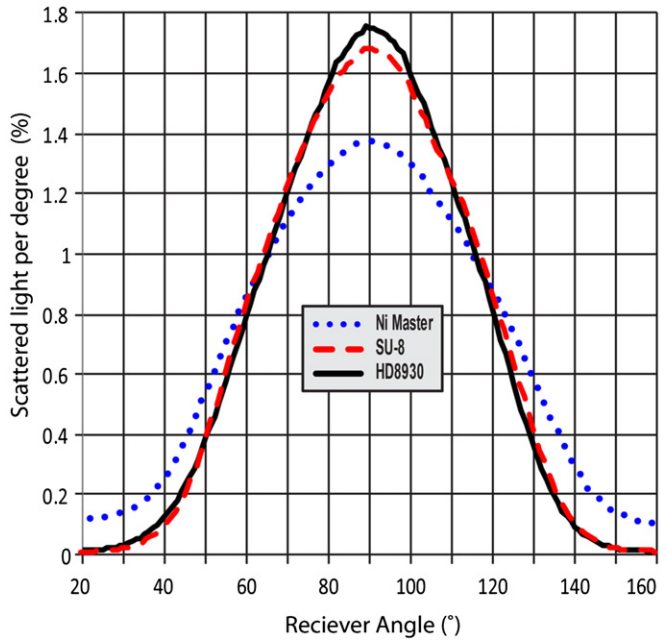


Figure 7. Angular reflection profile of reflective diffusers at different steps in the process: (*a*) master mold (*b*) SU-8 mold before crosslinking (*c*) final HD8930 membrane which closely matches the profile of the SU-8 mold after crosslinking (not shown). All surfaces were coated with aluminum before measurement.

using a servo motor with an integrated encoder to drive the rotation stage and by synchronously reading data from a digital photometer. The surfaces were coated with 100 nm evaporated aluminum. The nature of the reflector allows us to disregard whether or not the surface structure is inverted as the reflection distribution will be equivalent in either configuration. The resulting measurements for the three major stages in fabrication are presented in figure 7. It is important to note that the data in figure 7 is the reflection distribution in air. The reflection distribution of the final device will be more diffuse due to refraction of light when exiting the device.

The measured values were divided by the total area under each curve in order to allow for equal comparison of the distributions for each sample. To compare the distributions quantitatively, the standard deviations of each curve was calculated and is given in table 1. If the texture peak-to-valley height decreases, it is expected that the surface reflection becomes more mirror like and therefor a smaller standard deviation is expected over the normal distribution. The PDMS

Table 1. Standard deviation of reflectance distributions at critical process points.

Measurement point	Standard deviation (°)
Original Ni mold	2.07
SU-8 mold after post exposure bake	1.89
SU-8 mold after hard bake	1.85
HD8930 after release from mold	1.84

mold step has been omitted from the measurement due to difficulty in obtaining a high quality aluminum coating on the surface, however literature suggests that PDMS replication by this process should see no loss.

The majority of the pattern loss is seen in the transfer from the PDMS daughter to the SU-8 Master. This loss is likely due to the compression of the PDMS stamp during lamination. Reducing the compressive force during lamination could lessen the pattern loss, but lower pressure results in air trapping between the PDMS and SU-8 and therefore cannot be used. An additional heating step can be added after lamination to allow the uncured SU-8 to reflow to the uncompressed PDMS and improve pattern transfer, however this additional step often results in separation of the mold from the substrate due to unmatched thermal expansion coefficients between glass substrate and PDMS mold [16]. Further experimentation is required to determine the correct heat cycle to assure proper pattern transfer without mold separation. Alternately, the texture in the original Ni mold could be exaggerated to the degree that pattern loss results in the targeted level of surface texturing.

A loss was also seen due to shrinkage of the SU-8 during the final crosslinking of the SU-8 mold [8]. No significant pattern loss was seen due to any of the remaining processes. Further optimization of the replication process will be required to properly transfer the microstructured surface through to the final film, however, for this report, the transferred pattern was sufficient to demonstrate a device with a paper-like appearance (figure 4).

4.5. Pore scaling

For scalability to applications where smaller pores are desired such as higher resolution displays or micro-filtration membranes, a thinner membrane may be required. The process as described here is limited by a minimum path length of the UV light dictated by the membrane thickness. For sufficiently thick layers as shown here, the difference in UV transmission through the HD8930 and SU-8 is high and the process allows the UV to expose only the area above the high transmission material. However, as Beer-Lamberts law ($T = e^{-l\alpha_1}$ where T is the transmission through a layer and α is the absorption constant in the medium) states, the difference in transmission will be insignificant if the film must be made thinner in order to accommodate smaller pores. There should exist a minimum exposure ratio, TR_{min}, between the high and low absorption resists for the process to be successful, $T_1/T_2 = e^{-l(\alpha_1-\alpha_2)} > TR_{min}$. With fuller knowledge of the material properties, the value of TR_{min} could be determined and the minimum value

of l could be determined, however this work is left to future reports.

Though transmission ratios below TR_{min} were not encountered in this research, a possible solution to such an issue should be discussed. In order to improve TR_{min} in the process described here, a shift in exposure wavelength could be utilized. The absorption coefficient of hard baked SU-8 remains relatively low at wavelengths down to 300 nm while the absorption coefficient of typical HD8930 precursor increases dramatically as wavelength decreases below 365 nm [17, 18]. Therefore, with thinner HD8930 films, UV wavelength used during the membrane exposure step could be shifted below 365 nm to take advantage of the larger difference in absorption coefficients, thus allowing higher resolution pores to be fabricated. Alternately, UV absorbing dyes could be added to the HD8930 resist to increase the UV absorption and to improve TR_{min}.

Some applications may also require larger pore sizes, however there is also likely a maximum pore size which is compatible with this process. The process presented here relies on a difference between the thickness of the photoresist layer on the post features and the layer away from the post features. As shown in section 3.2 and quantified by other researchers, the thickness of the photoresist layer above the mold feature is dependent on the width of the feature [19]. Therefore a maximum pore diameter must exist, however this value has not been determined as it would require further knowledge of the photoresist development rate verses exposure energy as well as the wavelength specific absorption of all layers. Further experimentation to determine this value is left to future work.

5. Conclusion

We have shown a technique for fabricating highly designed, high strength, polymer, microfluidic membranes with integrated optical substructures. Though the technique shown here was developed for a specific application, it is anticipated that these processes could be utilized in a number of related applications in the fields of MEMS, microfluidics, and membrane sciences. Further development of this process will be needed to reduce pattern loss in the mold transfer step. Furthermore, exploration of through hole aspect ratios much beyond approximately 1:1 has not yet been made, but would be of interest to this particular project as well as other membrane applications. Even in cases where surface texturing is not required, this technique offers a method for generating highly uniform pore structures in high strength polymers using a single mask-less photolithography step.

References

[1] Hagedon M, Yang S, Russell A and Heikenfeld J 2012 Bright e-paper by transport of ink through a white electrofluidic imaging film *Nature Commun.* **3** 1173

[2] De Jong J, Lammertink R G H and Wessling M 2006 Membranes and microfluidics: a review *Lab Chip* **6** 1125–39

[3] Burggraaf A J and Cot L 1996 *Fundamentals of Inorganic Membrane Scienceand Technology* vol 4 (Amsterdam: Elsevier)

[4] Calvo J I, Hernandez A, Pradanos P, Martınez L and Bowen W R 1995 Pore size distribution in microporous membranes *J. Colloid Interface Sci.* **176** 467–78

[5] Apel P 2001 Track etching technique in membrane technology *Radiat. Meas.* **34** 559–66

[6] Ebrahimi Warkiani M *et al* 2013 Isoporous micro-/nano-engineeredmembranes *ACS Nano* **7** 1882–904

[7] Worgull M 2009 *Hot Embossing: Theory and Technology of Microreplication* (William Andrew Pub)

[8] Cannistra A T and Suleski T J 2010 Characterization of hybrid molding and lithography for SU-8 micro-optical components *J. Micro/Nanolithography, MEMS, MOEMS* **9** 013025

[9] Frieder Mugele B and Christophe J 2005 Electrowetting: from basics to applications *J. Phys.: Condens. Matter.* **17** R705

[10] Yang S, Zhou K, Kreit E and Heikenfeld J 2010 High reflectivity electrofluidic pixels with zero-power grayscale operation *Appl. Phys. Lett.* **97** 143501

[11] Yang S, Hagedon M and Heikenfeld J 2011 Light out-coupling for reflective displays: simple geometrical model, MATLAB simulation, and experimental validation *Disp. Technol. J.* **7** 473–7

[12] Heikenfeld J, Drzaic P, Yeo J-S and Koch T 2011 Review paper: a critical review of the present and future prospects for electronic paper *J. Soc. Inf. Disp.* **19** 129–56

[13] Youn S-W, Noguchi T, Takahashi M and Maeda R 2008 Fabrication of micro mold for hot-embossing of polyimide microfluidic platform by using electron beam lithography combined with inductively coupled plasma *Microelectron. Eng.* **85** 918–21

[14] Bertsch A, Lorenz H and Renaud P 1999 3D microfabrication by combining microstereolithography and thick resist UV lithography *Sensors Actuators* A **73** 14–23

[15] Han M, Lee W, Lee S-K and Lee S S 2004 3D microfabrication with inclined/rotated UV lithography *Sensors Actuators* A **111** 14–20

[16] Kunnavakkam M V *et al* 2003 Low-cost, low-loss microlens arrays fabricated by soft-lithography replication process *Appl. Phys. Lett.* **82** 1152–4

[17] Hsu S L-C and Chen W-C 2002 A novel positive photosensitive polybenzoxazole precursor for microelectronic applications *Polymer* **43** 6743–50

[18] Reznikova E F, Mohr J and Hein H 2005 Deep photo-lithography characterization of SU-8 resist layers *Microsyst. Technol.* **11** 282–91

[19] White L K 1986 Spun-on contour coating characterizations for advanced optical lithography *Polym. Eng. Sci.* **26** 1135–9